Experimental and Computational Multiphase Flow
Vol. 6, No. 2, 2024, 135–139
https://doi.org/10.1007/s42757-023-0173-y

3D simulation of pulsatile bubbly flow resembling decompression sickness conditions inside a realistic human artery

Sotiris P. Evgenidis (✉), Thodoris D. Karapantsios

Chemical and Environmental Technology Lab, Department of Chemical Technology and Industrial Chemistry, School of Chemistry, Aristotle University of Thessaloniki, Thessaloniki GR-54124, Greece

Abstract

I-VED (*In-Vivo* Embolic Detector) is a novel diagnostic tool for non-invasive, real-time detection of bubbles in humans. Bubbles are precursors of decompression sickness (DCS), which can be encountered in astronauts, scuba divers, etc. I-VED exploits an EU patented electrical impedance spectroscopy technology, developed under the umbrella of a European Space Agency project. So far, I-VED has been calibrated and validated *in vitro*. In view of the forthcoming *in-vivo* trials, it needs to be configured for sensing bubbles in the bloodstream. For this, 3D computational fluid dynamics simulation is performed to investigate axial and radial variation of void fraction (α) and flow velocity (U) in a pulsatile bubbly flow inside a realistic human artery (diameter: 5–20 mm, implying vessel dilatation or contraction), where liquid velocity, bubble size, and void fraction resemble DCS conditions. Results show that U and α show a core-peaking profile despite the variation of artery diameter, while 3D sharp turns yield U and α non-uniformities in the angular direction that do not affect mean void fraction across the artery. Obtained knowledge allows deeper insight on the physics and spatial characteristics of bubbly flow in a real artery, which is useful in the design of measuring volume and tuning of I-VED.

Keywords

computational fluid dynamics (CFD)
bubbly flow
decompression sickness (DCS)
void fraction
flow velocity

Article History

Received: 6 September 2022
Revised: 7 May 2023
Accepted: 24 July 2023

Research Article

1 Introduction

Decompression sickness (DCS) results from the formation of bubbles as soon as environmental pressure decreases below the sum of inert gas partial pressures (usually nitrogen) dissolved in blood and body tissues. Rapid reduction of environmental pressure that overcomes the rate of inert gas washout from the blood and tissues increases the risk of DCS incidents considerably (Makowski et al., 2022). DCS is commonly classified as type 1 or type 2. Type 1 DCS is characterized by musculoskeletal pain and mild cutaneous symptoms. On the other hand, Type 2 DCS symptoms are more serious and fall into three categories: neurological, inner ear, and cardiopulmonary complications (Yanagawa et al., 2021). Activities that pose a risk for DCS include extra-vehicular activities (EVAs) of astronauts outside the spacecraft, working in caisson, underwater diving decompression, and flying in unpressurized aircraft (Zueco and López-González, 2016).

Doppler ultrasonography is the most common method for monitoring decompression-induced bubbles. However, differentiation between bubble-generated sounds and background sounds, e.g., from the moving blood cells at peak flow during the systolic phase of the heartbeat, can be difficult and, as a result, both acquisition and interpretation of Doppler audio signals are highly operator dependent (Chappell and Payne, 2005; Møllerløkken et al., 2016). In addition, ultrasound clinical systems are currently incompatible with a low-cost, wearable, continuous imaging approach and this limits their use for field data collection (e.g., during EVAs of astronauts and underwater diving) (Le et al., 2021). Bio-impedance technology, which is applied in different medical applications (e.g., for the detection of bladder cancer and the measurement of cardiac stroke volume), is considered suitable enough to overcome the abovementioned limitations of ultrasound imaging (Aroom et al., 2009). On the one hand, the compatibility of bio-impedance technology with wearable devices is already mature enough and, on the

✉ sevgenid@chem.auth.gr

other hand, bio-impedance sensors do not require any special experience and training of the operator. Moreover, bio-impedance signals can be recorded continuously during an activity (e.g., EVA and diving) and, furthermore, it is feasible to conduct simultaneous measurements at different parts of the human body applying several pairs of electrodes of proper size, shape, and geometry (Nebuya et al., 2011).

Computational fluid dynamics (CFD) modelling offers in-depth understanding of multiphase flow physics and, as a result, improves the design and operation of employed multiphase flow measurement techniques. To the best of our knowledge, literature lacks CFD studies on DCS induced bubbly flow in human arteries. Instead, a number of numerical studies have investigated the parameters (viscosity, gravity, pressure, surface tension, etc.) which affect bubble dynamics in human vasculature when employing gas embolotherapy method to treat vascularized solid tumors, where bubble size is comparable to the artery diameter (slug flow) (e.g., Ye and Bull, 2004; Poornima and Vengadesan, 2012; Salajeghe and Saidi, 2022). Additionally, it is worth noticing that Evgenidis and Karapantsios (2022) recently performed 2D CFD simulations to study the case of pulsatile bubbly flow in a column that approximates the flow inside human vena cava during DCS.

The present authors and their colleagues in the School of Chemistry at the Aristotle University, Greece, have developed an EU patented electrical impedance spectroscopy technique (EP 3005942 A1, 2016) for non-invasive, real-time bubble detection in human arteries and consequently DCS diagnosis, under the umbrella of the European Space Agency Project "*In-Vivo* Embolic Detector, I-VED" (Contract No. 4000101764, 2004–2014). This novel diagnostic tool has been calibrated and validated with the aid of a bench top flow-loop that accommodated electrical, optical, pressure, and acoustical diagnostics and provided well-controlled bubbly flow where liquid velocities, bubble sizes, and void fractions resembled DCS conditions (Evgenidis et al., 2010; Evgenidis and Karapantsios, 2015, 2018a, 2018b; Gkotsis et al., 2019, 2020). *In-vitro* testing of I-VED has shown that it can: (1) detect even a-few-micron bubbles in a liquid flow, (2) sense void fraction fluctuations down to 10^{-5}, and (3) calculate average bubble size of a gas–liquid flow from the intensity of electrical signal fluctuations. In order to examine next the performance of the novel technology *in vivo*, I-VED system needs to be carefully configured, aiming to sense bubbles present in the bloodstream. For this, 3D CFD simulation is performed in this study to investigate for the first time both axial and radial variations of void fraction and flow velocity in a pulsatile bubbly flow that resembles DCS inside a realistic human artery. It allows deeper insight into the physics and spatial characteristics of two-phase blood flow with sub-millimeter bubbles in a real artery geometry, which is useful in the design of the measuring volume and tuning of I-VED. Next, a 3D CFD approach is briefly described and then results are obtained, presented, and discussed.

2 Method

3D simulation of pulsatile bubbly flow resembling DCS conditions inside a realistic artery is performed by means of the commercially available CFD code ANSYS 2019-R3. To do this, a 3D computational grid consisting of 36,418 hexahedral elements and corresponding to a realistic right coronary artery is developed based on Berthier et al. (2002) (Fig. 1). The length of the vessel is 500 mm, while its diameter varies from 5 to 20 mm, implying vessel dilatation or contraction. The lower values of this range correspond to typical diameters of several human vessels (e.g., jugular vein), while the higher one is close to the diameter of human vena cava (21 mm) where bubbles gather during a decompression incident (Vann et al., 2011). Bubbly flow inside the artery is modelled applying the Eulerian multiphase model. This is the most complex one; however, it is considered tractable enough for such flows by averaging the equations in space. The two phases are assumed as interpenetrating and interacting continua, and separate momentum and mass balance equations are solved for each phase. This approach benefits from the convenient two-way coupling between phases (Mohammadi et al., 2019).

Liquid and gas properties as well as conditions used for the 3D simulation are listed in Table 1. Physical properties were taken at body temperature 37 °C. Liquid viscosity and density (assuming Newtonian behavior) simulate blood physical properties (Woodcock, 1976). Employed input cross-sectional mean liquid velocity, $U_{l,mean}$ = 0.03 m/s, is representative of bloodstream in human vena cava (Vann et al., 2011). Reynolds number of single liquid phase ranges

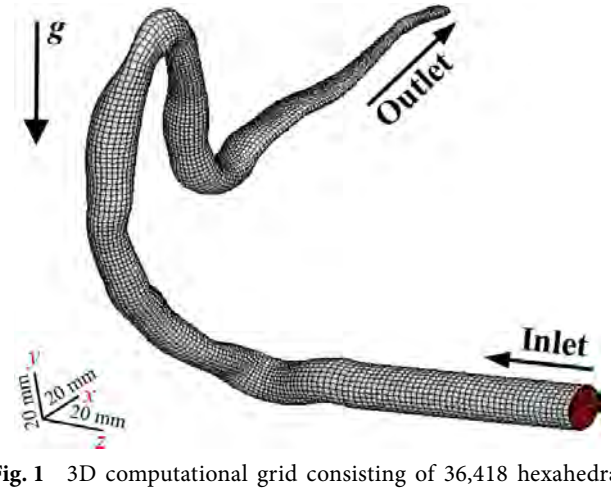

Fig. 1 3D computational grid consisting of 36,418 hexahedral elements that corresponds to a realistic right coronary artery.

Table 1 Liquid–gas properties at 37 °C and conditions used in 3D simulation

Parameter	Value
Liquid density (kg/m^3)	1050
Liquid viscosity (mPa·s)	4.5
Gas density (kg/m^3)	1.225
Gas viscosity (mPa·s)	1.79×10^{-2}
Gravitational acceleration (m/s^2)	9.81
Cross-sectional mean liquid velocity, $U_{l,mean}$ (m/s)	0.03
Sinusoidal pulsation frequency, f (Hz)	1
Sinusoidal pulsation amplitude, A (% of $U_{l,mean}$)	50
Bubble diameter, D_b (μm)	300
Cross-sectional mean void fraction, α_{mean}	0.03
Total time of simulation (s)	1.0

from 35 to 140 for varying artery diameter (5–20 mm) and corresponds to laminar flow. Pulsatile liquid flow is simplified to a sinusoidal flow profile with frequency (f) of 1 Hz (corresponding to 60 heart beats per minute, which is a typical resting/reference heart rate for adults) and amplitude (A) ±50% of average flow rate (Brandt et al., 2021). Combining all the above, inlet flow velocity $U(t)$ is given by the functional form in Eq. (1):

$$U(t) = U_{l,mean} + AU_{l,mean}\sin(2\pi ft) \quad (1)$$

Gas physical properties correspond to air for simplicity. A mono-disperse bubble size distribution of sub-millimeter bubbles, D_b = 300 μm, as well as a cross-sectional mean void fraction value, α_{mean} = 0.03, both typical for severe DCS conditions, are used as input parameters in the simulation. A gravity term is also included to account for the buoyancy of the bubbles.

3 Results

Obtained results from the 3D simulation of pulsatile bubbly flow inside the right coronary artery are shown in Figs. 2(a), 2(b), and 3. Figure 2(a) shows streamlines colored by flow velocity (U) magnitude. For an input cross-sectional mean liquid velocity of 0.03 m/s, U varies from ~0 (close to the artery walls) to ~0.7 m/s (at the center of the artery in the case of stenosis). Additionally, Fig. 2(b) presents representative flow velocity profiles at different cross-sections of the artery. At these cross-sections, Fig. 3 displays the relevant void fraction (α) profiles aiming to identify void fraction extreme values across and along the vessel in an effort to facilitate I-VED system configuration. For an input cross-sectional mean void fraction of 0.03, α ranges radially from ~0.02 (close to the artery walls) to ~0.04 (close to the center of the artery), but shows insignificant variation in the axial

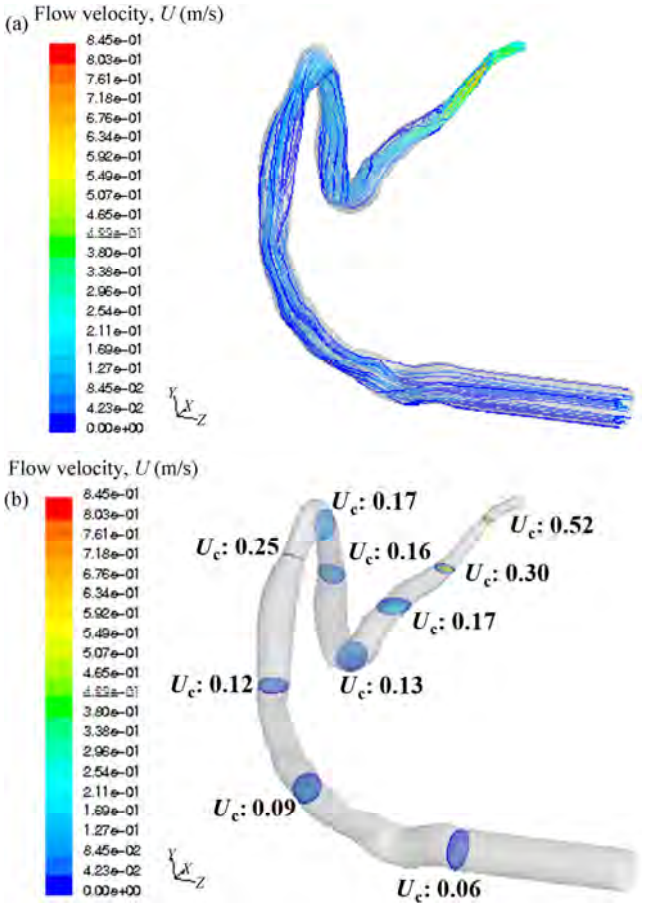

Fig. 2 3D simulation of pulsatile (sinusoidal) bubbly flow inside a realistic right coronary artery: (a) streamlines coloured by flow velocity (U) magnitude, (b) flow velocity (U) profiles accompanied with the respective cross-sectional mean U values (U_c) at various cross sections. Input data: α_{mean} = 0.03, $U_{l,mean}$= 0.03 m/s, pulsation frequency 1 Hz, pulsation amplitude ±50%, D_b = 300 μm.

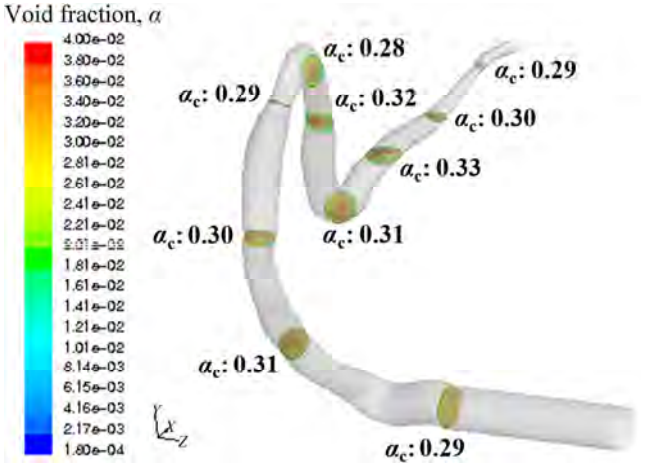

Fig. 3 3D simulation of pulsatile (sinusoidal) bubbly flow inside a realistic right coronary artery: void fraction (α) profiles accompanied with the respective cross-sectional mean α values (α_c) at various cross sections. Input data: α_{mean} = 0.03, $U_{l,mean}$ = 0.03 m/s, pulsation frequency 1 Hz, pulsation amplitude ±50%, D_b = 300 μm.

direction. In general, both flow velocity and void fraction demonstrate a core-peaking profile despite the variation of artery diameter. This behavior for sub-millimeter bubbles under such special conditions is noteworthy since this type of profile is commonly encountered for bubbles larger than 4 mm (Song et al., 2001). Previous experimental and drift–flux model findings of the authors for similar (steady) flow conditions validate the outcome of 3D simulation (e.g., Evgenidis and Karapantsios, 2018a, 2018b; Gkotsis et al., 2019). It is interesting to note that the 3D sharp turns yield some void fraction and flow velocity non-uniformities in the angular direction; however, they do not seem to affect the mean void fraction across the artery. This quantity does not show any remarkable variation due to artery stenosis (decrease of vessel diameter) either, as a result of flow velocity increase.

4 Discussion

I-VED is a novel and highly-sensitive electrical impedance spectroscopy technique for non-invasive detection of bubbles in humans. So far, I-VED has been calibrated and validated *in vitro*. In view of the forthcoming *in-vivo* trials, 3D simulation of pulsatile bubbly flow resembling DCS conditions inside a realistic artery contributes to I-VED system adaptation as follows.

- Void fraction seems to vary across the artery about ±30% with respect to the input mean α value. This means that for the extreme case of void fraction value around 0.05, α will vary from 0.035 to 0.065. Therefore, considering the measured electrical impedance value of the vessel under investigation in the absence of bubbles, I-VED electronics need to be properly tuned in order to achieve the maximum sensitivity for void fraction values lower than 0.1.
- Since void fraction varies across the artery indicating generally a core-peaking profile with some non-uniformities in the angular direction, I-VED shall focus on the determination of the mean void fraction across the vessel under study. To do this, the electrical equivalent of the system needs to be carefully considered to impose an electric field distribution through the entire cross-section of the measuring artery. In doing so, the critical parameters to be defined are the dimensions and distance of electrodes attached to the skin (Fig. 4). Electrode dimensions affect the measurement sensitivity and signal intensity, while the distance between the electrodes dictates the measuring volume of the technique (Devia and Fossa, 2003; Evgenidis and Karapantsios, 2015). Vessels surrounded by thinner (partially conductive) subcutaneous tissue will be preferentially examined first for convenience (e.g., radial and ulnar artery in the forearm), although I-VED is not sensitive to the depth of the artery under study since electrical measurements in the presence of bubbles are normalized against the baseline measurement (in the absence of bubbles).
- I-VED enables simultaneous measurements at different sites of the human body. Mean void fraction seems unaffected by vessel diameter; however, it would be interesting to measure synchronously and compare void fraction in vessels where bubbles usually appear during DCS (jugular vein-neck, popliteal vein-lower limb, vena cava-trunk) (Vann et al., 2011). As concerns the determination of mean bubbly flow velocity by cross-correlating different I-VED signals, vessel diameter shall be taken into serious consideration. Flow velocity increases in smaller vessels and the distance between the electrode pairs shall be carefully defined to provide intense peak correlation and adequate sensitivity to estimate time lag as well.

All in all, 3D simulation facilitates I-VED system configuration and, consequently, reduces the number of the necessary *in-vivo* trials.

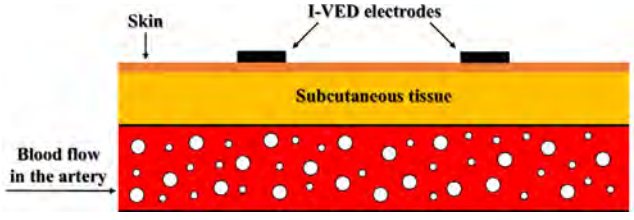

Fig. 4 Conceptual design for non-invasive sensing of bubbles present in a human artery by attaching I-VED electrodes to the skin.

Funding note

Open access funding provided by HEAL-Link Greece.

Acknowledgements

The authors are really thankful to Mr. Vangelis Skaperdas for his contribution in performing CFD simulations. This study was funded by ESA GSTP Project: *In-Vivo* Embolic Detector, I-VED - Contract No. 4000101764. The view expressed herein can in no way be taken to reflect the official opinion of the European Space Agency.

Author contributions

SE carried out the simulation, performed data analysis, and wrote the manuscript. TK coordinated and supervised the activities, took over the acquisition of financial support for the project, and reviewed the manuscript.

Declaration of competing interest

The authors have no competing interests to declare that are relevant to the content of this article.

References

Aroom, K. R., Harting, M. T., Cox, C. S., Radharkrishnan, R. S., Smith, C., Gill, B. S. 2009. Bioimpedance analysis: A guide to simple design and implementation. *Journal of Surgical Research*, 153: 23–30.

Berthier, B., Bouzerar, R., Legallais, C. 2002. Blood flow patterns in an anatomically realistic coronary vessel: Influence of three different reconstruction methods. *Journal of Biomechanics*, 35: 1347–1356.

Brandt, A. H., Olesen, J. B., Moshavegh, R., Jensen, J. A., Nielsen, M. B., Hansen, K. L. 2021. Common carotid artery volume flow: A comparison study between ultrasound vector flow imaging and phase contrast magnetic resonance imaging. *Neurology International*, 13: 269–278.

Chappell, M. A., Payne, S. J. 2005. A method for the automated detection of venous gas bubbles in humans using empirical mode decomposition. *Annals of Biomedical Engineering*, 33: 1411–1421.

Devia, F., Fossa, M. 2003. Design and optimisation of impedance probes for void fraction measurements. *Flow Measurement and Instrumentation*, 14: 139–149.

Evgenidis, S. P., Karapantsios, T. D. 2015. Effect of bubble size on void fraction fluctuations in dispersed bubble flows. *International Journal of Multiphase Flow*, 75: 163–173.

Evgenidis, S. P., Karapantsios, T. D. 2018a. Gas–liquid flow of sub-millimeter bubbles at low void fractions: Experimental study of bubble size distribution and void fraction. *International Journal of Heat and Fluid Flow*, 71: 353–365.

Evgenidis, S. P., Karapantsios, T. D. 2018b. Gas–liquid flow of sub-millimeter bubbles at low void fractions: Void fraction prediction using drift–flux model. *Experimental Thermal and Fluid Science*, 98: 195–205.

Evgenidis, S. P., Kazakis, N. A., Karapantsios, T. D. 2010. Bubbly flow characteristics during decompression sickness: Effect of surfactant and electrolyte on bubble size distribution. *Colloids and Surfaces A: Physicochemical and Engineering Aspects*, 365: 46–51.

Evgenidis, S., Karapantsios, T. 2022. Pulsatile gas–liquid flow resembling decompression sickness: Computational fluid dynamics simulation and experimental validation. *International Maritime Health*, 73: 189–198.

Gkotsis, P. K., Evgenidis, S. P., Karapantsios, T. D. 2019. Influence of Newtonian and non-Newtonian fluid behaviour on void fraction and bubble size for a gas–liquid flow of sub-millimeter bubbles at low void fractions. *Experimental Thermal and Fluid Science*, 109: 109912.

Gkotsis, P. K., Evgenidis, S. P., Karapantsios, T. D. 2020. Associating void fraction signals with bubble clusters features in co-current, upward gas–liquid flow of a non-Newtonian liquid. *International Journal of Multiphase Flow*, 131: 103297.

Le, D. Q., Dayton, P. A., Tillmans, F., Freiberger, J. J., Moon, R. E., Denoble, P., Papadopoulou, V. 2021. Ultrasound in decompression research: Fundamentals, considerations, and future technologies. *Undersea & Hyperbaric Medicine*, 48: 59–72.

Makowski, M. S., Sproul, C., Swartz, C., Everitt, J. I., Knaus, D. A., Wilbur, J. C., Moon, R. E. 2022. Safety evaluation of carbon tetrafluoride as an inert hyperbaric breathing gas in Sprague–Dawley rats. *Toxicology and Applied Pharmacology*, 444: 116023.

Mohammadi, M. H., Sotiropoulos, F., Brinkerhoff, J. R. 2019. Eulerian–Eulerian large eddy simulation of two-phase dilute bubbly flows. *Chemical Engineering Science*, 208: 115156.

Møllerløkken, A., Blogg, S. L., Doolette, D. J., Nishi, R. Y., Pollock, N. W. 2016. Consensus guidelines for the use of ultrasound for diving research. *Diving and Hyperbaric Medicine*, 46: 26–32.

Nebuya, S., Mills, G. H., Milnes, P., Brown, B. H. 2011. Indirect measurement of lung density and air volume from electrical impedance tomography (EIT) data. *Physiological Measurement*, 32: 1953–1967.

Poornima, J., Vengadesan, S. 2012. Numerical simulation of bubble transport in a bifurcating microchannel: A preliminary study. *Journal of Biomechanical Engineering*, 134: 081005.

Salajeghe, R., Saidi, M. S. 2022. Investigation of the different parameters contributing to bubble sticking inside physiological bifurcations. *Medical & Biological Engineering & Computing*, 60: 599–618.

Song, Q., Luo, R., Yang, X., Wang, Z. 2001. Phase distributions for upward laminar dilute bubbly flows with non-uniform bubble sizes in a vertical pipe. *International Journal of Multiphase Flow*, 27: 379–390.

Vann, R. D., Butler, F. K., Mitchell, S. J., Moon, R. E. 2011. Decompression illness. *Lancet*, 377: 153–164.

Woodcock, J. P. 1976. Physical properties of blood and their influence on blood-flow measurement. *Reports on Progress in Physics*, 39: 65–127.

Yanagawa, Y., Takeuchi, I., Ishiyama, J. 2021. Ultrasound in the diagnosis of acute-phase decompression sickness. *Radiology Case Reports*, 16: 698–700.

Ye, T., Bull, J. L. 2004. Direct numerical simulations of micro-bubble expansion in gas embolotherapy. *Journal of Biomechanical Engineering*, 126: 745–759.

Zueco, J., López-González, L. M. 2016. Network model to study physiological processes of hypobaric decompression sickness: New numerical results. *Acta Astronautica*, 121: 256–270.